Chapter 5

Seasonal and Diurnal Variations of Vertical Profile of Precipitation over Indonesian Maritime Continent

Marzuki, Hiroyuki Hashiguchi, Mutya Vonnisa and Harmadi

Additional information is available at the end of the chapter

http://dx.doi.org/10.5772/intechopen.74044

Abstract

This chapter presents variabilities in the vertical structure of precipitation over the Indonesian maritime continent (IMC), which were inferred from the gradients of the radar reflectivity (dBZ) below the freezing level and were gathered from the latest 2A25 TRMM–Precipitation Radar product over a 17-year time span (1998–2014). In general, the downward increasing (DI) pattern of dBZ toward the surface is more dominant than the downward decreasing (DD) pattern, which has a ratio of 1.3. The DI is frequently observed over the ocean, and the higher prevailing rain top heights over land are associated with DD, in most cases. Shallow convective rains have the largest ratio of DI to DD (>4), followed by deep convective rains. The largest ratio is observed during December–January–February (DJF) when wetter conditions are dominant over the IMC, which is a favorable condition for raindrop growth. The stratiform rains show a dominant DD in which the ratio of DD to DI is greater than 1.6 for each season. The spatial distribution of the stratiform gradient is more complex than that of convective rain and does not show a robust land-ocean contrast. The diurnal variation in the reflectivity gradient for stratiform rain is less pronounced. With convective rain, DD is more dominant in the afternoon and evening over a large island, indicates a decrease in the raindrop concentration due to the evaporation and updraft associated with the intense convection.

Keywords: radar reflectivity gradient, Indonesian maritime continent, TRMM, seasonal variation, diurnal variation

1. Introduction

The precipitation pattern over the Indonesian maritime continent (IMC) is very unique due to a complex interaction between the local and global scale atmospheric circulations. The IMC

consists of thousands of islands, which range in size from less than 1 km to several thousands of kilometers. The complex shape, geography, and orientation of the island coastlines contribute to the uniqueness of the IMC environment (**Figure 1a**). In addition to the complex geographical variation, precipitation formation in the IMC involves large-scale atmospheric circulations such as El Niño–Southern Oscillation (ENSO) [1, 2], Madden-Julian Oscillation (MJO) [3, 4], and monsoons. The local circulation such as the diurnal cycle of precipitation [5] may be modified by larger-scale circulation [6, 7], and thus, the precipitation pattern over the IMC becomes more complex. The IMC receives a large amount of rainfall throughout the year, and precipitation varies considerably across the region [8–10]. The average annual rainfall at several locations is very high and can reach 6200 mm (**Figure 1b**). The lightning activity also varies from one region to another with the annual lightning ground flash density of 97 fl $km^{-2}yr^{-1}$ in certain locations (**Figure 1c**). Heavy rainfall in this region often leads to numerous hazards that result in high economic losses.

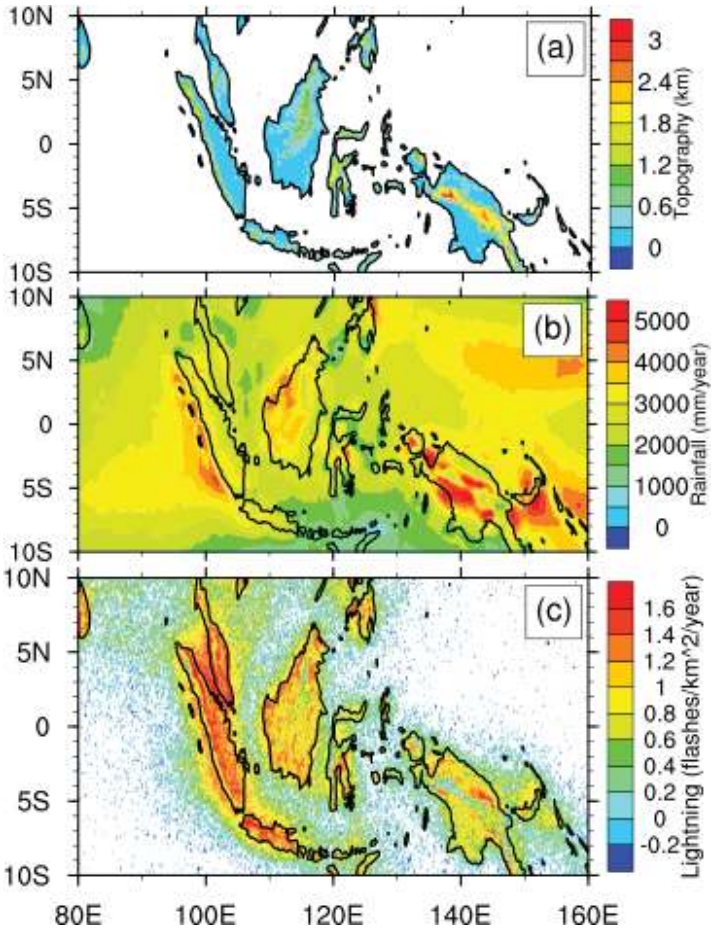

Figure 1. Topography (a), mean annual rainfall from TRMM 3B43 during 1998–2015 (b) and lightning from the TRMM LIS during 1998–2013 (c), over the IMC. Lightning colorbar is in log scale.

http://dx.doi.org/10.5772/intechopen.74044

Complex interactions between the local and global scale atmospheric circulations during precipitation formation in the IMC are the most challenging issues regarding rainfall estimates, weather prediction, and climate modeling [11]. However, research on the variability of Indonesian tropical precipitation has been primarily focused on the spatial and temporal variability of surface rainfall and less focused on the vertical profile of precipitation. This is despite knowledge of the vertical structure of precipitation being an important aspect in cloud dynamics and thermodynamics, which includes latent heating and remote sensing algorithm development. Vertical heating profiles from the stratiform (convective) precipitation process in the upper (lower) portion of the clouds [12] control the atmospheric circulation. Apart from the bright band near melting layer, the increase (decrease) in the rainfall rate toward the surface in stratiform clouds indicates the growth (evaporation) of precipitating particles because of microphysical processes [13]. The evaporation that occurs during the precipitation cycle of water plays an important role in the horizontal and vertical transport of energy in the atmosphere [14]. In remote sensing technology, vertical precipitation profiles are required for developing rain retrieval algorithms, which are used for satellite microwave measurements because the top of the atmosphere brightness temperatures vary depending upon the vertical structure of precipitation even though the rainfall rates at the surface are the same [15]. Furthermore, most operation ground-based radar cannot measure rainfall close to the surface. Thus, information about the vertical gradient of the rainfall rate below the freezing level is crucial for the estimation of surface rainfall.

Given the significant implications of the precipitation vertical profile, many subsequent studies have been performed. There have been numerous reports of spatiotemporal variation in the precipitation vertical profile over Asia or larger areas [15–19]. For a smaller climatic region, there have also been some studies completed in Africa [20], India [21], and the Huaihe River Basin in China [22]. However, comprehensive analysis of the statistical properties of precipitation vertical profile over the IMC has not yet been found. Some previous studies are only based on the data obtained from several locations, particularly in Java and Sumatra. Previous studies are mostly deal with the characteristics of raindrop size distribution (DSD) [9, 23–25], the diurnal and intraseasonal variations in precipitation [4, 26]. Thus, in this chapter, the first study to investigate the precipitation vertical profile for the entire IMC region is presented.

2. Theoretical background

In this chapter, the vertical profile of precipitation over the IMC was revealed from the radar reflectivity gathered by precipitation radar (PR) onboard the tropical rainfall measuring mission (TRMM) satellite. Therefore, prior to discussing the data and methodology, we will briefly review the physical basis of radar reflectivity.

Precipitation radar uses the returned radio waves from water drops and ice crystals in the troposphere to estimate the precipitation rate. The returned power (P_r) and characteristics of the radar and target can be expressed in an equation called the radar equation, which is given by the following:

$$P_r = \frac{C}{r^2} Z \tag{1}$$

where r is the distance from the radar to the target, C is a constant depending on the radar equipment, and Z is the radar reflectivity factor, which is determined by the physical properties of the target. The returned power and radar reflectivity factor are usually expressed in decibels (dB) because they span a large range of values. Therefore, dBZ is the unit most frequently seen on the radar display, which stands for decibel relative to Z and can be estimated by solving Eq. (1) as follows:

$$10\log(Z) = 10\log(P_r) + 20\log(r) - 10\log(C) \tag{2}$$

The dBZ is a basic quantity used in weather radar. Radar reflectivity (Z) is an inherent property of a raindrop, which is given by the following:

$$Z = \int N(D)\, D^6\, dD \tag{3}$$

where D is the raindrop diameter and $N(D)$ is raindrop size distribution. Eq. (3) is only valid if the radar wavelength is larger than the raindrop size, which is also known as Rayleigh scattering. On the other hand, if the wavelength (λ) is not large enough compared with the raindrop size, then the radar reflectivity equation as follows:

$$Z = \frac{\lambda^4}{\pi^5 |K_w|^2} \int \sigma(D) N(D) dD \tag{4}$$

where σ is the Mie scattering cross section and $|K_w|$ is the complex index of refraction for water [27].

Weather radar has become essential in cloud physics, weather observation, and forecasting. Accurate estimates of both the spatial and temporal distribution of observed rainfall are important inputs for weather forecasts, river and flash flood models, and others. Unfortunately, the accuracy of rainfall estimates using weather radar is affected by multiple sources of error. The errors originate from the internal characteristics of weather radar such as the miscalibration of radar parameters in constant C of Eq. (2). Other error sources are from external environmental conditions such as ground clutter, partial beam blockage, signal attenuation, and the vertical profile of radar reflectivity. Most operation, ground-based radar cannot measure radar reflectivity close to the surface. The minimum effective height of radar coverage may be 1–2 km or more above the surface [18]. Thus, information about the vertical gradient of radar reflectivity below freezing level is crucial for the estimation of the surface radar reflectivity.

Radar reflectivity is proportional to the sixth power of the drop size (Eq. (3)), and thus, the characteristics of a raindrop have a disproportionate effect on radar reflectivity. Downward increasing or decreasing of radar reflectivity toward the surface is related to the evolution of raindrop, particularly a large-sized drop. Over the IMC, spatiotemporal variation of DSD is clearly observed, particularly for heavy rains [9, 23–25]. As the physical properties of precipitation, such as raindrops, continuously change and vary spatially and temporally due to many aspects, the vertical gradient of radar reflectivity also varies. Therefore, using a fixed vertical gradient of radar reflectivity values can result in erroneous surface reflectivity that leads to erroneous rainfall estimates from weather radar. However, a study on the vertical profile of precipitation over the IMC remains limited to several locations.

Once the surface radar reflectivity is available, this value must be converted to the desired parameter, which is rainfall rate (R), by using the Z-R relationship obtained from the raindrop measurement. However, as explained above, considerable spatiotemporal variation in DSD is well documented. Thus, the inappropriate selection of Z-R relation is another source in weather radar. To reduce this conversion error, many radars use rain gauge networks although this technique is difficult to use for extreme rainfall measurements [28]. Detailed discussion of the variability of raindrop size distribution and Z-R relationship is beyond the scope of this chapter.

3. Data and methodology

In this chapter, attenuation corrected equivalent radar reflectivity from the TRMM PR 2A25 data product was used. The 2A25 has level 2 algorithms from TRMM PR, which generate products associated with radar signal processing and physical processes of storms. The TRMM PR works in the Ku band frequency with horizontal resolutions of 4.3 and 5.7 km at nadir, before and after boost, respectively [29]. The vertical resolution is 250 m with the total number of vertical range gate of 80. The height corresponds to the distance measured along the radar beam from the point of intersection between the beam and Earth's ellipsoid, and this is not to the local vertical height.

In the current study, the TRMM PR V7 data for a time span of more than 17 years, from 1998 to 2014, is examined. The PR consists of 49 angle bins with an angle-bin interval of 0.71°, which gives a maximum scan angle of 17° about the central beam. However, because the focus of this study is on vertical structure and a reduction of problems at higher scan angles is sought, such as like range-height offset, only the profiles with an incidence angle of less than 7° on either side of nadir are included, which is similar to some of the previous studies [20, 21].

The PR has a minimum sensitivity of approximately 17 dBZ [29]. In this study, only those reflectivity profiles with a $Z \geq 17$ dBZ for at least seven consecutive range bins are considered. Also excluded from this study is the virga profile, where only the profile with detectable surface rainfall is analyzed. The vertical profile of radar reflectivity gradient (VPRG) is used to express the vertical gradient of precipitation. The gradient is calculated by using the linear regression as a function of dBZ and height. Negative values indicate a downward decreasing (DD) of radar reflectivity toward the surface, which is characterized a maximum rainfall rate aloft and positive rates denotes a downward increasing (DI) pattern. The gradient is calculated for the dBZ profile below the freezing level (0.75–3 km) with four consecutive range bins [18].

Separation radar reflectivity profile between convective and stratiform is important in precipitation study because each rain type is characterized by different mechanisms of precipitation growth. The TRMM PR V7 of 2A25 classifies the rain type into more than 30 subcategories which can be summarized into several major types: stratiform, stratiform maybe, convective, convective maybe, and others [30]. Simply, the bright band (BB) signature is used to identify the stratiform and convective. If BB is not detected, and yet, any value of radar reflectivity in the beam exceeds 39 dBZ, the profile is labeled convective. Furthermore, if BB is not detected, and the convective reflectivity threshold is not met, the profile is called other. In this study, only those reflectivity profiles with stratiform and convective labels are considered. The convective reflectivity profiles are then classified into deep and shallow convective. The profile

with a rain top height (RTH) of less than the freezing level height is considered to be shallow rain; otherwise it is assumed to be deep convective. In this work, the RTH is assumed to be at the highest altitude with $Z \geq 18$ dBZ for at least two consecutive range bins.

Of the many variations in precipitation over the IMC, characteristics of the vertical profile of radar reflectivity at seasonal and diurnal scales are the main focus of this chapter. The seasons are classified into four categories, that is, December, January, February (DJF); March, April, May (MAM); June, July, August (JJA); and September, October, November (SON). Using the aforementioned database, the spatiotemporal distribution of profile number, mean gradient and RTH are contoured on 0.25 × 0.25° boxes. Mean gradient and RTH is only calculated if the number of profiles in that box is more than three.

4. Results

4.1. Climatology of vertical profile of precipitation

Figure 2a shows the climatology of the number of reflectivity profiles for a time span of more than 17 years, from 1998 to 2014. Approximately 27,075,680 profiles have been used to generate this contour. The most dominant profile was observed in the oceans, especially in the Indian and Pacific Oceans. In addition, a rather high profile number is also observed in some parts of Borneo. The largest number of profiles is approximately 4000, and the smallest is approximately 100. A relatively small number of profiles are observed in the oceans in the southern part of Indonesia, especially in the eastern region. Thus, the largest number of profiles observed in the two warm oceans, that is, Indian and Pacific Oceans, are consistent with the climatology of annual rainfall (**Figure 1**).

In general, the DI of radar reflectivity toward the surface is more dominant than the DD pattern. The most dominant DI was observed in the Indian Ocean, whereas DD was observed on land (**Figure 2b**). This is evident from the larger ratio of DI to DD in the oceans than on land. The largest ratio of DI to DD is approximately 6, and the smallest ratio is 0.66. This value does not change much for the extreme gradient (gradient > ± 1 dBZ/km), in which the smallest ratio is 0.64 and the largest is 5.61 (**Figure 2c**). The dominant DI pattern in the ocean, which indicates a significant raindrop growth was previously found by some investigators [15–18]. Because DI is more dominant in the oceans, the mean gradient of reflectivity in the oceans is more positive than on land (**Figure 2d**). The gradient pattern seems to strongly coincide with the rain top height. A higher RTH is more frequently observed on land than in the oceans (**Figure 2e**). The largest ratio of RTH > 5 km to RTH < 5 km is approximately 6.2 and the smallest is 0.47. This RTH ratio value is nearly equal to the ratio of DI to DD.

4.2. Seasonal variation of vertical profile of precipitation

Prior to discussing the seasonal variation of the precipitation vertical profile, in this section, the seasonal variations in low level relative humidity (RH) are first provided (**Figure 3**). Active periods of convection over the IMC are observed during DJF, which is associated with a dominant westerly wind. During this period, wet conditions (RH >70% at 850 hPa) are visible within the entire IMC region except in the eastern Pacific Ocean. During MAM, the humidity

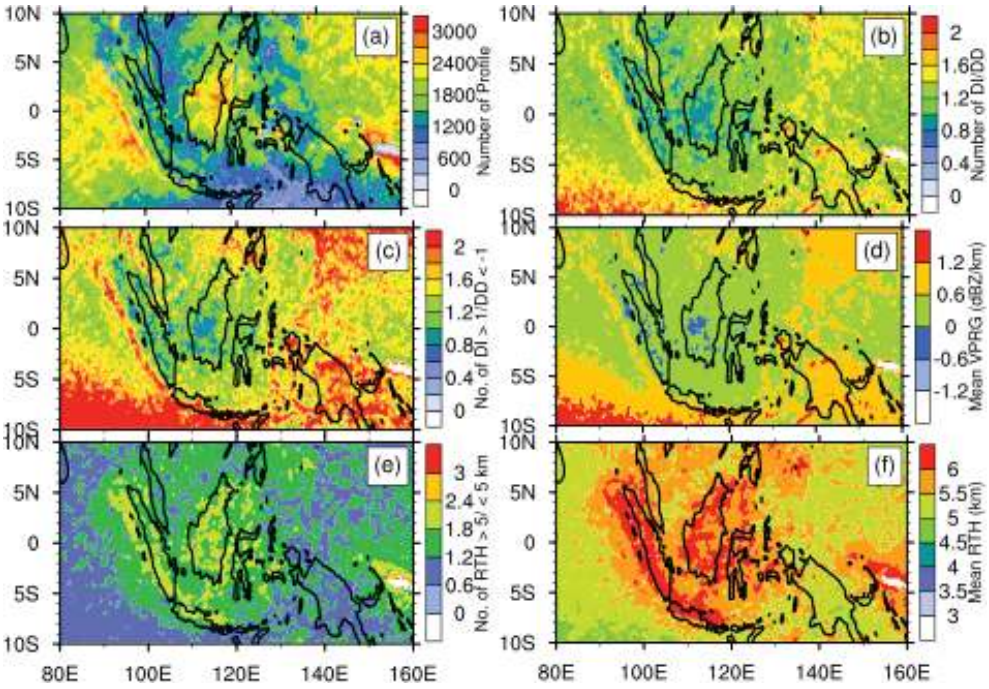

Figure 2. Climatology of rain profile (a), ratio of radar reflectivity profiles with gradient greater than 0 (DI) to profiles with gradient less than 0 (DD) (b), ratio of radar reflectivity profiles with extreme gradient greater than 1 (DI > 1) to profiles with extreme gradient less than 1 (DD < 1) (c), mean radar reflectivity gradient (d), ratio of radar reflectivity profiles with rain top height (RTH) greater than 5 km to profiles with RTH less than 5 km (e) and mean RTH (f). The diagram was calculated in the 0.25 × 0.25° grids.

is slightly high over land, which means that convection over land is active. On the other hand, a slightly high humidity is observed over Papua and the Pacific Ocean during JJA. November is a rainy season in some parts of western IMC, and a slightly high relative humidity was observed over this region. In general, an inactive convection period over the IMC is associated with prevailing easterly winds [30].

Figure 4 shows the monthly variation in the number of radar reflectivity profiles, ratio of DI to DD, mean VPRG and mean RTH for each rain type. Percentage of profiles is calculated by normalizing the profile in one-month bins. The largest percentage of profiles occurs in December and January, which is consistent with convection period over the IMC (**Figure 3**). The largest ratio of DI to DD was also observed during these months, followed by June, July and August. The smallest percentage of profiles was seen in August, which is the dry season over the IMC. All rain types exhibit similar percentage patterns. The gradient is more positive in January and December. On the other hand, the mean rain top height is lower during this period. Thus, mean reflectivity gradient pattern is contrary to the rain top height, which is discussed above (**Figure 2**).

To see the spatial variation in the radar reflectivity profile, the spatial distribution of the ratio of DI to DD, mean of VPRG and RTH for deep, shallow and stratiform are given in **Figures 4–6**, respectively. For the entire dataset (without rain type classification), the ratio of DI to DD for DJF,

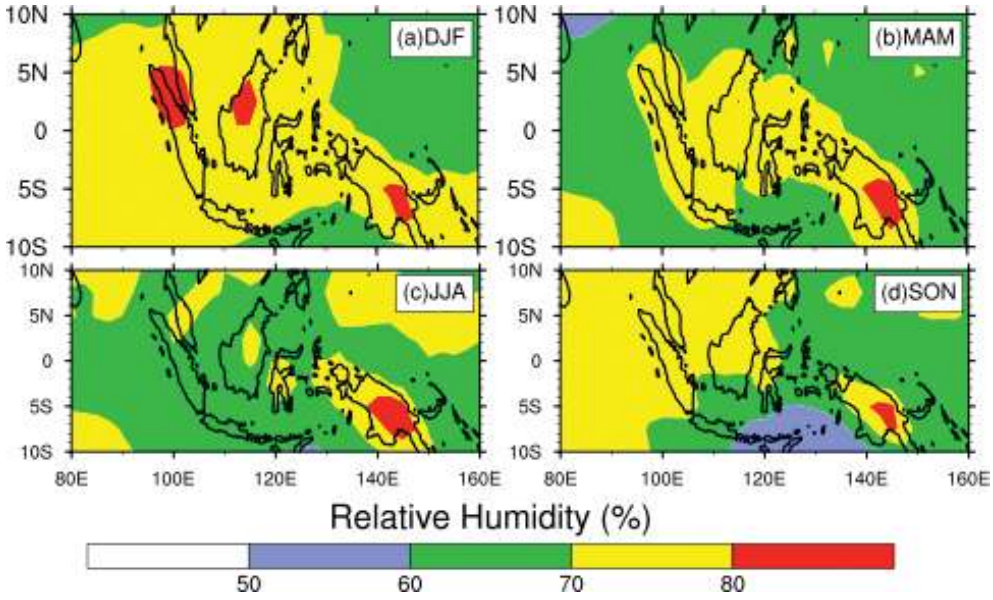

Figure 3. Seasonal variation of relative humidity at 850 hPa from the National Centers for atmospheric prediction (NCEP) and the National Center for Atmospheric Research (NCAR) reanalysis data.

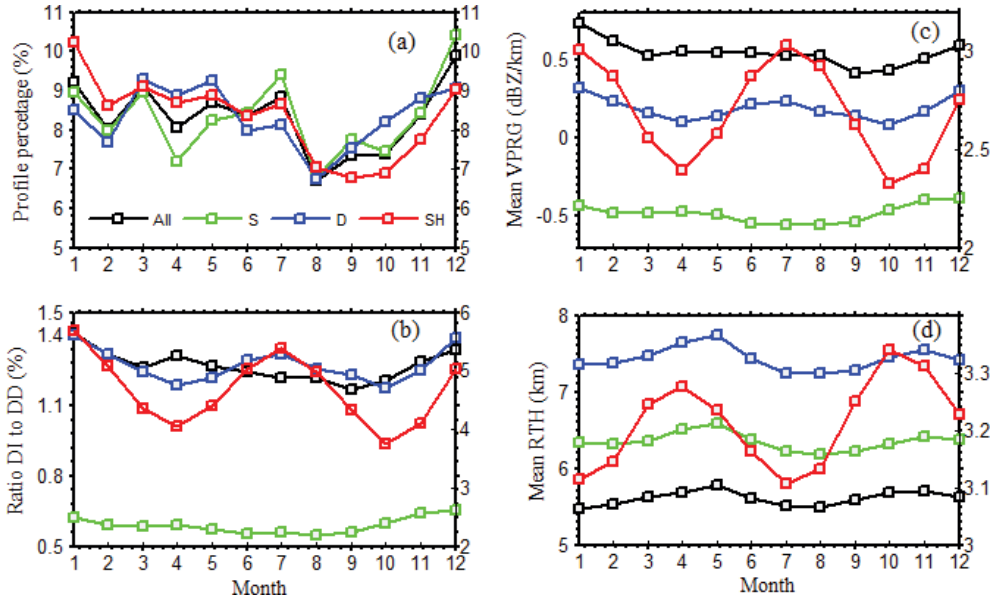

Figure 4. Monthly variation of percentage of radar reflectivity profile (a), ratio of DI to DD (b), mean VPRG (c) and mean RTH (d). Symbols of S, D and SH indicate stratiform, deep and shallow convective, respectively. Left y axis is used for shallow convective rain.

MAM, JJA, and SON are 1.36, 1.28, 1.23, and 1.22, respectively. Deep convective has a slightly dominant DI with the ratio of DI to DD being 1.37, 1.22, 1.30, and 1.22, respectively. Moreover, the shallow convective rain has a larger ratio, in which the ratio for each season is 5.27, 4.26, 5.13, and 4.05, respectively. In contrast to convective rain, stratiform rain has a more dominant DD in which the ratio of DD to DI for DJF, MAM, JJA, and SON are 1.60, 1.71, 1.80, and 1.66, respectively. Thus, in terms of the profile number, there is an increase in DI percentage during DJF and JJA, except for stratiform rain. This is also visible in the dual peak in **Figure 4**. In general, Indonesia has three rain zones with different rainfall peaks (see **Figure 3** of [31]). The first zone includes south Sumatera to Timor island, southern Kalimantan, and Sulawesi with a DJF peak. The second zone has a rainfall peak in MAM and October, November, and December, which includes northwest Indonesia from northern Sumatra to northwestern Kalimantan. The last region includes Maluku and northern Sulawesi with a rainfall peak during June and July. Because **Figure 4** was averaged in the area covering all three rain zones, two dominant peaks are observed during November, December, January (first peak) and June and July (second peak).

The DI is more dominant in deep convective rain than DD (**Figure 5**) with the previously described ratio. This indicates significant raindrop growth. Convection generally has stronger updrafts, which can modify the drops through drop sorting and enhancement of the collision–coalescence process. Both processes will increase the concentration of medium and larger-sized drops, the former by not allowing the smaller drops to fall and the latter by consuming the smaller drops. The study of the vertical profile of DSD using wind profiler radar and Micro Rain Radar (MRR) over Sumatera proves this hypothesis [3, 23, 33]. A slightly larger downward increasing of deep convective reflectivity gathered from wind profiler radar is consistent with the low-level raindrop growth, which is inferred by the MRR observation.

In general, the DI pattern is dominant in the ocean, particularly during wet conditions (DJF). A wetter environment may be a favorable condition for raindrop growth. During MAM, JJA and SON, the gradient becomes more negative, especially between the longitude of 100 and 120° E. High relative humidity values over large islands during this period do not cause DI of radar reflectivity toward the surface. On land, the growth of the raindrops by the collision–coalescence process was much less efficient [34]. During the active convection (DJF), westerly winds blow from the Indian Ocean. Therefore, the precipitation systems over large islands such as Sumatera and Borneo are more maritime in nature than those present during the active convective period. The propagation of clouds from brightness temperature data indicates this phenomenon. Furthermore, the precipitation over land during the inactive convection period particularly in MAM and JJA, is characterized by deeper storms (**Figure 5j** and **k**), which is common with continental rain [3]. **Figure 5j** and **k** reinforce the terrain effect on the reflectivity gradient in deep convective rain, which has been reported in some previous studies [32].

Figure 6 shows the seasonal variation of the precipitation vertical profile for shallow convective. In general, the pattern of shallow convective is the same as that of deep convective. The DI over the ocean is also more dominant than over land. A more positive gradient over land was observed during MAM and JJA (**Figure 6f** and **g**), which is coincident with a higher rain top height (**Figure 6j** and **k**). However, the ratio of DI to DD for shallow convective is much larger than deep convective. Thus, the raindrop growth during shallow convective rains is

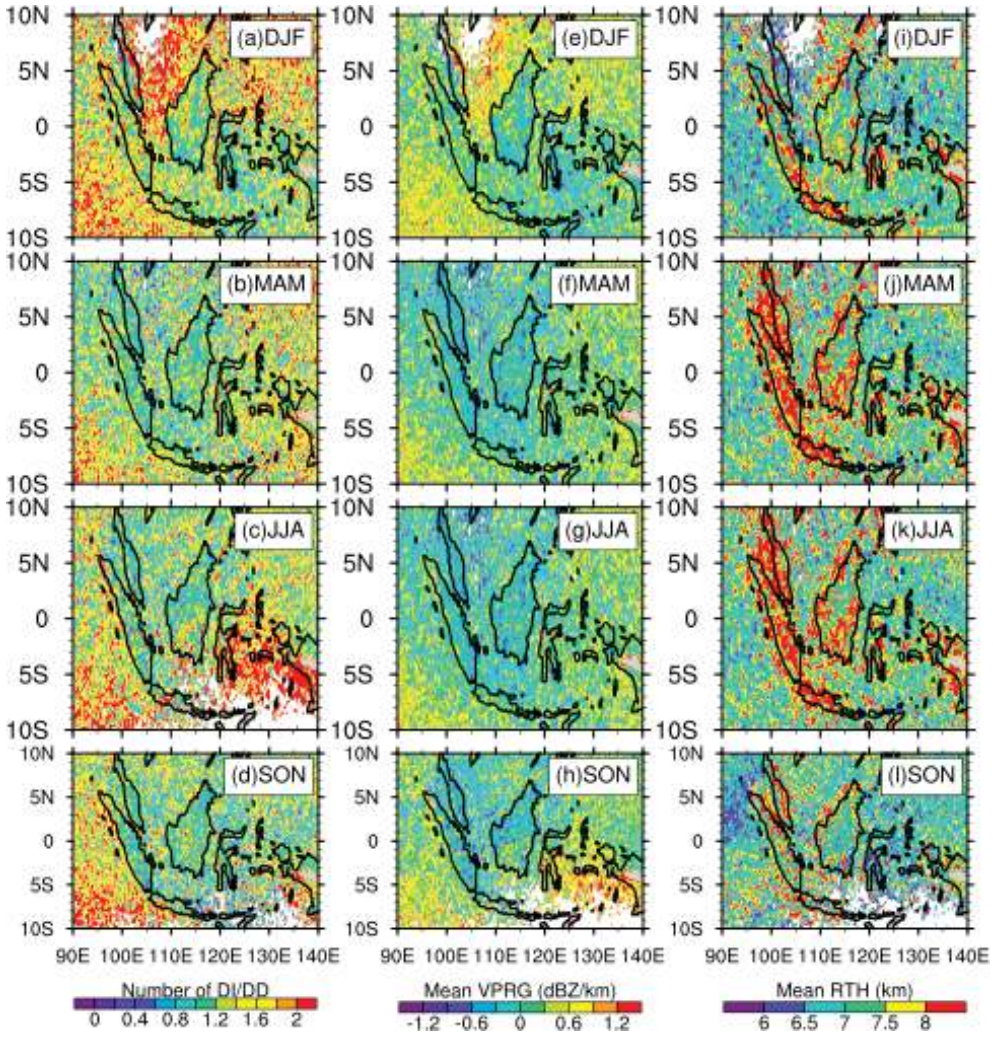

Figure 5. Seasonal variation of the ratio of DI to DD (left), mean VPRG (middle) and mean RTH (c) for deep convective rains.

more significant than deep convection. In addition to the collision–coalescence process due to the convective updraft, two other processes determine raindrop growth, that is, accretion of bulk cloud water and self-collection among raindrops [35]. The updraft is generally weaker over ocean than over land [36]. The strength of the updrafts affects the height at which collisions between different sized droplets occur. A strong updraft (more common over land) will not allow the smaller drops to fall until the particles are large enough to fall. Therefore, a greater concentration of small-sized-raindrops will be observed at the surface. On the other hand, smaller raindrops can fall and monotonically grow in weaker updraft condition [36]. Therefore, the value of DI in convective rain, including shallow convective, is larger over the ocean than over land.

http://dx.doi.org/10.5772/intechopen.74044

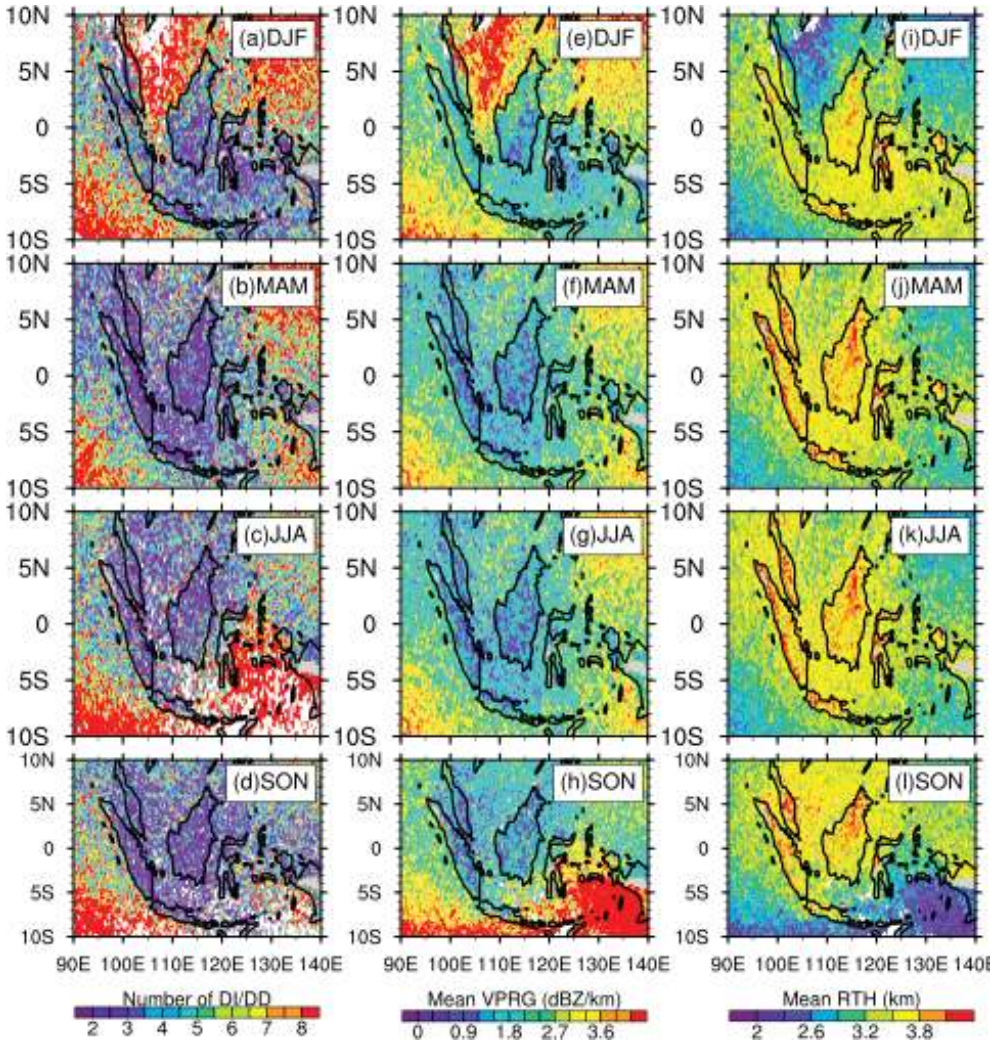

Figure 6. Same as **Figure 5**, but for shallow convective rain.

For stratiform, DD is more dominant than DI, which indicates a reduction of raindrop concentration toward the surface due to the evaporation process [13]. While the DD is dominant, some profiles also show a DI pattern. Moderate and heavy rain intensity during stratiform rain is associated with DI or less negative DD [32].

The spatiotemporal distribution of the reflectivity gradient for stratiform rain does not show a significant seasonal variation (**Figure 7**). The land-sea contrast is not clearly observed for this rain. Thus, the effect of terrain appears to be negligible for stratiform rain, which was previously found in another region [32]. This result supports the previous study on the characteristics of DSD over the IMC. The DSD over the IMC, particularly in Kototabang (Sumatera) and Singapore, shows much less seasonal variation than in India, especially for light (stratiform) rain [24, 33].

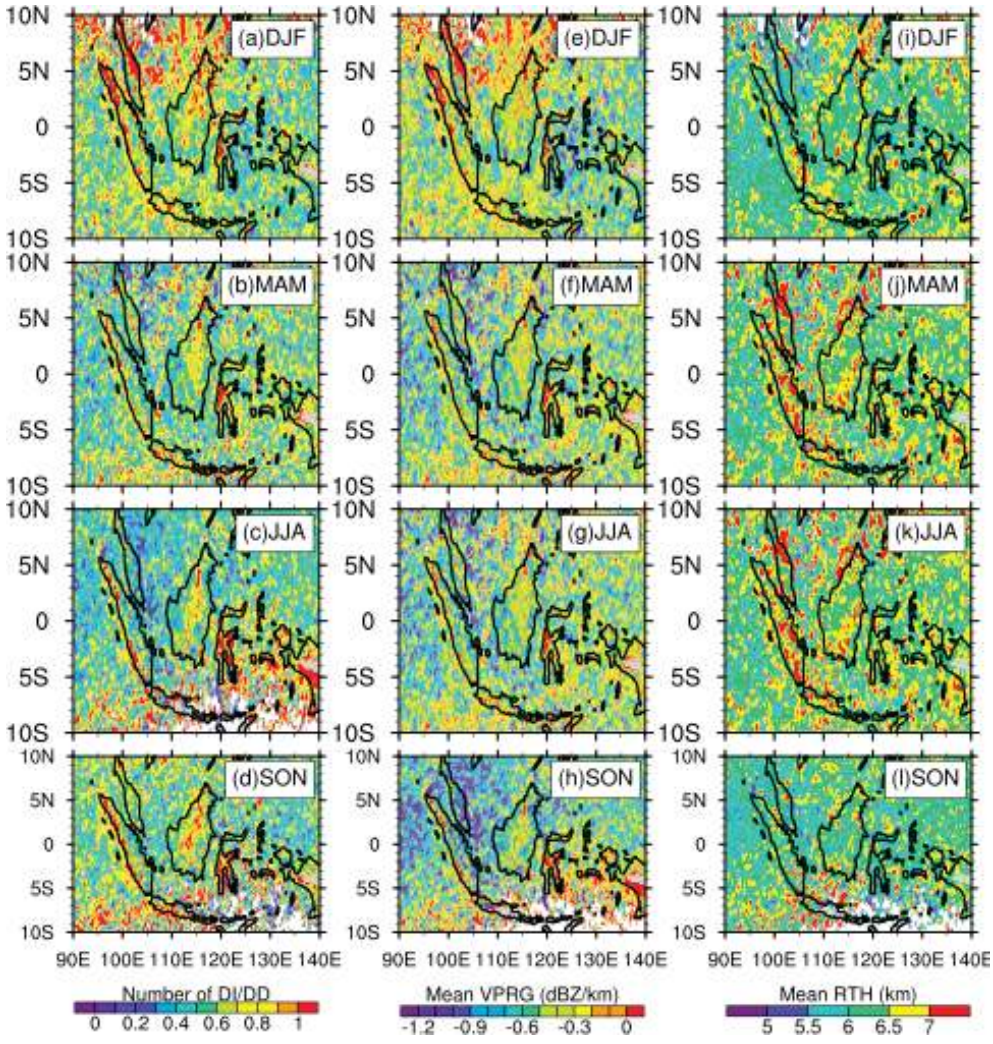

Figure 7. Same as **Figure 5**, but for stratiform rain.

4.3. Diurnal variation of radar reflectivity gradient

The diurnal cycle of precipitation is a prominent mode over the IMC. There have been many studies on the diurnal variation of surface rainfall over the IMC [3, 5, 7, 11], and the focus here is on the diurnal variation of precipitation vertical profile.

Figure 8 shows the diurnal cycle of the number of radar reflectivity profiles for each rain type. From the early morning until morning, that is, 01-06 local time (LT), the number of profiles on land is very small, especially for deep and shallow convective rains. Simultaneously, many stratiform profiles are observed in the coastal region of Sumatra and surrounding seas. In addition, the amount of stratiform rain is also widely observed around the coastal region of Papua.

http://dx.doi.org/10.5772/intechopen.74044

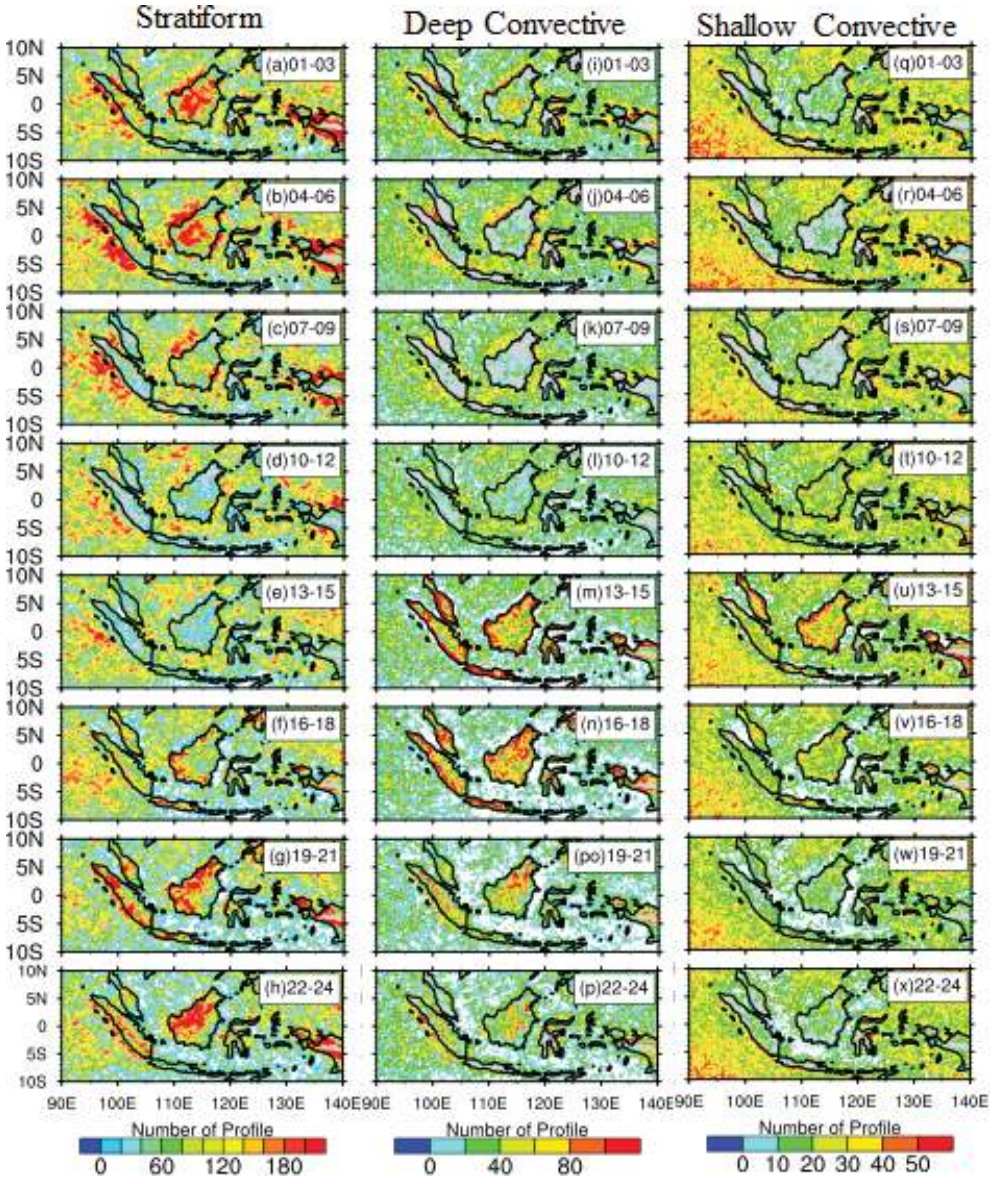

Figure 8. Diurnal variation of profile number for stratiform (left), deep (middle), and shallow convective rains (right).

The large number of shallow convective profiles is also widely observed in the Indian Ocean, especially in the southern region between 01 and 09 LT. From 13 LT, the number of convective profiles on land increases and reaches a peak between 16 and 18 LT. For shallow convective rain, the largest number of profiles on land is observed between 13 and 15 LT. On the other hand, the peak of stratiform profile numbers on land is observed rather later than the convective rain, namely, between 19 and 24 LT. During this period, the number of profiles in the ocean

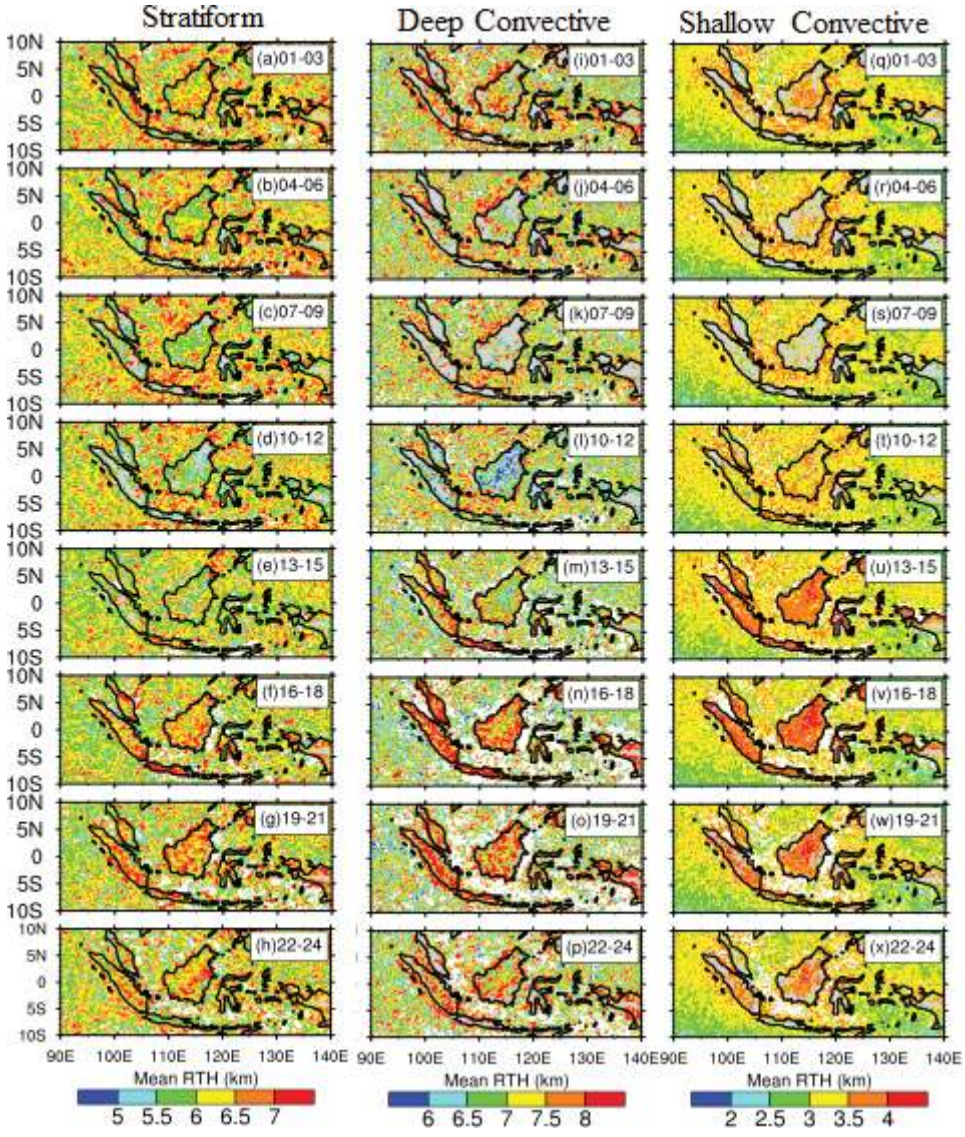

Figure 9. Same as **Figure 8** but for rain top height.

is suppressed.Based on **Figure 8**, when the convective rain profile reaches a peak in the afternoon over land, the stratiform profile number is at a minimum during this period. Furthermore, when the stratiform profile reaches a peak in the ocean during the early morning, the convective rain profile is at a minimum over land. Migration of the evening convection over land and early morning convection over ocean has been described previously in some papers [5].

http://dx.doi.org/10.5772/intechopen.74044

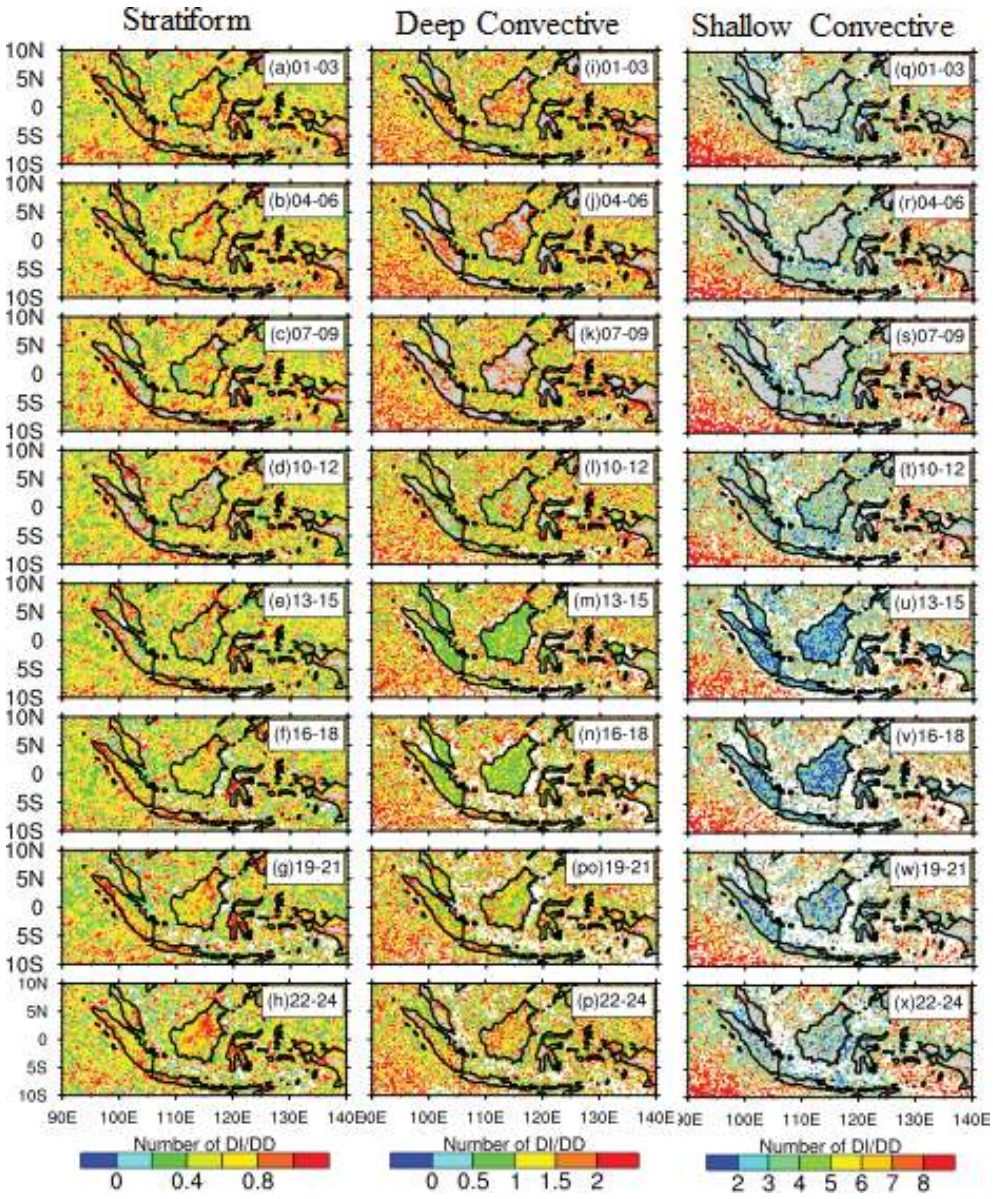

Figure 10. Same as **Figure 8** but for the ratio of DI to DD.

Mature convection over land is normally a result of surface solar heating and a gravity wave forced by convection. Land-based convection is associated with high rain top height due to a strong updraft. This can be seen in **Figure 9**, in which between 13 and 21 LT, the rain top over

land is higher than during other time periods. On the other hand, over the ocean, the diurnal variation in rain top height is not obvious.

The diurnal cycle of the DI to DD ratio is similar to the rain top height pattern. The ratio of DI to DD over land is relatively small when the rain top height is high, namely, between 13 and 18 LT. For the entire dataset (without diurnal classification), ratio of DI to DD for 01–06 LT, 07–12 LT, 13–18 LT, and 19–24 LT are 1.30, 1.29, 1.25, and 1.25, respectively. Deep convective has a slightly dominant DI, with a ratio of DI to DD being 1.34, 1.31, 1.18, and 1.28, respectively. Moreover, the shallow convective rain has a larger ratio, in which the ratio for each hour is 4.99, 4.72, 4.22, and 4.77, respectively. On the other hand, the ratios for stratiform rain are 0.62, 0.60, 0.56, and 0.59, respectively (**Figure 10**).

The summary of the aforementioned discussion is given in **Figure 11**. Two major peaks are observed, in which one is over land and the other is over ocean. Furthermore, the rain top height increases with increasing time, particularly between 12 and 24 LT. During this period, the reflectivity gradient is less positive or more negative, which is an indication of the reduction of raindrops toward the surface due to evaporation, particularly small-sized raindrops. Disdrometer observations in Sumatera have shown that the raindrop spectra from noon to evening contains less small-sized drops (<2 mm) than at other hours [37]. Between 00 and 12 LT,

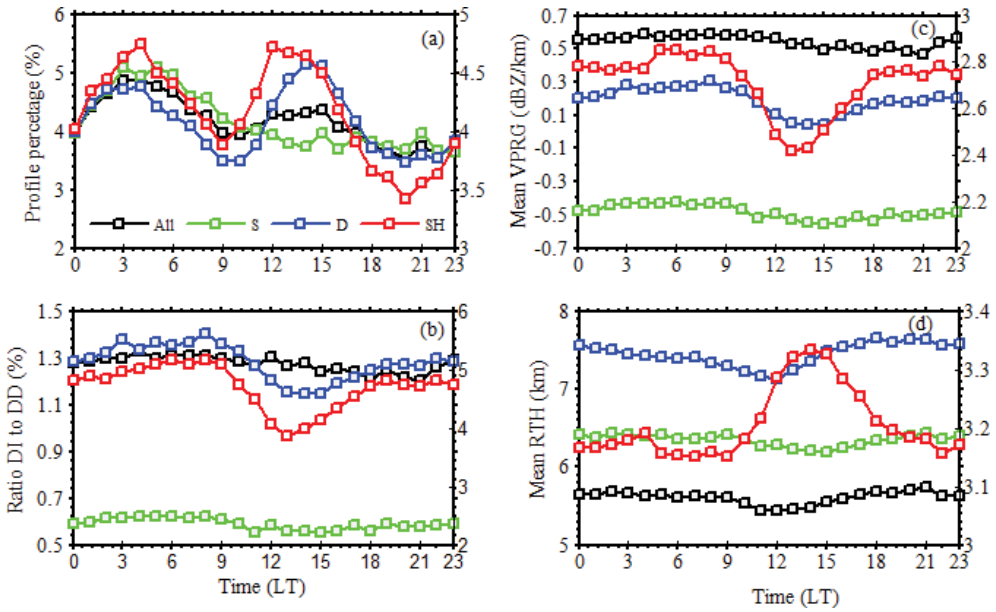

Figure 11. Diurnal variation of number of radar reflectivity profile (a), the ratio of DI to DD (b), mean VPRG (c), and mean RTH (d). Symbols of S, D and SH indicate stratiform, deep and shallow convective, respectively. Left *y* axis is for shallow convective rain.

the rain top height decreases, and the reflectivity gradient increases (**Figure 11c** and **d**), which indicates raindrop growth.

5. Conclusions

The vertical structure of radar reflectivity has many applications, but it has not been comprehensively analyzed on the IMC, which is a region with complex precipitation formation due to the interaction of local circulation dominantly affected by the topography and some global circulations. In this chapter, we present the statistical analysis of seasonal and diurnal variations of such a profile. The gradient is calculated using a linear regression of radar reflectivity as a function of height, in which the positive gradient is denoted as DI and the negative gradient is the DD of radar reflectivity toward the surface. In general, the pattern of reflectivity gradient in this work is similar to that previously found on a global scale, in which the dominant DI is observed in the oceans and DD is observed predominantly on land. However, the diurnal and spatial variations in the gradient shows interesting feature. For convective rainfall, the ratio of DI to DD increases during the wet season such as DJF, whereas during the drier season (MAM and JJA), the number of DD pattern increases, especially over land as the rain top height increases due to the prevailing land-based convection. The stratiform rain does not show a significant seasonal variation, which is consistent with some previous studies on the seasonal variation in raindrops over the IMC. The vertical structure of radar reflectivity shows significant diurnal variations, and the pattern is similar to the land-ocean convection migration, which has been previously reported in some studies. The smallest DI ratio, especially over land, is observed during intense solar radiation. This indicates the reduction of raindrop concentration due to evaporation, especially small-sized raindrops, which are seen from a deficit of such raindrops during this period. The results in this chapter will be useful for the quantitative estimation of rainfall based on weather radar, particularly over the IMC.

Acknowledgements

This work was supported by the 2017 International Joint Collaboration and Scientific Publication grant from the Ministry of Research, Technology and Higher Education of the Republic of Indonesia (Contract no. 02/UN.16.1.17/PP.KLN/LPPM/2017). The authors thank to Japan Aerospace Exploration Agency and Goddard Space Flight Center for providing the data particularly 2A25 V7 data.

Conflict of interest

There is no conflict of interest.

Author details

Marzuki[1]*, Hiroyuki Hashiguchi[2], Mutya Vonnisa[1] and Harmadi[1]

*Address all correspondence to: marzuki@fmipa.unand.ac.id

1 Department of Physics, Andalas University, Padang, Indonesia

2 Research Institute for Sustainable Humanosphere (RISH), Kyoto University, Kyoto, Japan

References

[1] Sprintall J, Gordon AL, Koch-Larrouy A, Lee T, Potemra JT, Pujiana K, Wijffels SE. The Indonesian seas and their role in the coupled ocean-climate system. Nature Geoscience. 2014;**7**:487-492. DOI: 10.1038/ngeo2188

[2] Lee HS. General rainfall patterns in Indonesia and the potential impacts of local seas on rainfall intensity. Watermark. 2015;**7**:1751-1768

[3] Marzuki, Hashiguchi H, Kozu T, Shimomai T, Shibagaki Y, Takahashi Y. Precipitation microstructure in different madden–Julian oscillation phases over Sumatra. Atmospheric Research. 2016;**168**:121-138

[4] Shibagaki Y, Shimomai T, Kozu T, Mori S, Fujiyoshi Y, Hashiguchi H, Yamamoto MK, Fukao S, Yamanaka MD. Multi-scale convective systems associated with an intraseasonal oscillation over the Indonesian maritime continent. Monthly Weather Review. 2006;**134**:1682-1696

[5] Mori S, Hamada JI, Tauhid YI, Yamanaka MD, Okamoto N, Murata F, Sakurai N, Sribimawati T. Diurnal rainfall peak migrations around Sumatera Island, Indonesian maritime continent observed by TRMM satellite and intensive rawinsonde soundings. Monthly Weather Review. 2004;**132**:2021-2039

[6] Hamada J-I, Mori S, Kubota H, Yamanaka MD, Haryoko U, Lestari S, Sristyowati R, Syamsudin F. Interannual rainfall variability over northwestern Jawa and its relation to the Indian Ocean dipole and el Niño-southern oscillation events. SOLA. 2012;**8**:69-72

[7] Hendon HH. Indonesian rainfall variability: Impacts of ENSO and local air–sea interaction. Journal of Climate. 2013;**16**:1775-1790

[8] As-syakurab AR, Tanaka T, Osawa T, Mahendra MS. Indonesian rainfall variability observation using TRMM multi-satellite data. International Journal of Remote Sensing. 2013;**34**(21):7723-7738

[9] Marzuki M, Hashiguchi H, Yamamoto MK, Mori S, Yamanaka MD. Regional variability of raindrop size distribution over Indonesia. Annales de Geophysique. 2013;**31**:1941-1948. DOI: 10.5194/angeo-31-1941-2013

[10] Yanto BR, Zagona E. Space–time variability of Indonesian rainfall at inter-annual and multi-decadal time scales. Climate Dynamics. 2016:1-15

[11] Sato T, Miura H, Satoh M, Takayabu YN, Wang Y. Diurnal cycle of precipitation in the tropics simulated in a global cloud-resolving model. Journal of Climate. 2009;**22**:4809-4826

[12] Tokay A, Short DA. Evidence from tropical raindrop spectra of the origin of rain from stratiform versus convective clouds. Journal of Applied Meteorology. 1996;**35**:355-371

[13] Fujiyoshi Y, Takasugi T, Gocho Y. Radar-echo structure of middle-level precipitating clouds and the change of raindrops-processes of mixing of precipitation particles falling from generating cells. Journal of the Meteorological Society of Japan. 1980;**58**:203-216

[14] Magagi R, Barros AP. Estimation of latent heating of rainfall during the onset of the Indian monsoon using TRMM PR and radiosonde data. Journal of Applied Meteorology. 2004;**43**:328-349. DOI: 10.1175/1520-0450(2004)043<0328:EOLHOR>2.0.CO;2

[15] Fu Y, Liu G. The variability of tropical precipitation profiles and its impact on microwave brightness temperatures as inferred from TRMM data. Journal of Applied Meteorology. 2001;**40**:2130-2143

[16] Hirose M, Nakamura K. Spatial and seasonal variation of rain profiles over Asia observed by space-borne precipitation radar. Journal of Climate. 2002;**15**:3443-3458

[17] Hirose M, Nakamura K. Spatial and diurnal variation of precipitation systems over Asia observed by the TRMM precipitation radar. Journal of Geophysical Research. 2005. DOI: 10.1029/2004JD004815

[18] Liu C, Zipser EJ. Why does radar reflectivity tend to increase downward toward the ocean surface, but decrease downward toward the land surface? Journal of Geophysical Research. 2013;**118**:135-148. DOI: 10.1029/2012JD018134

[19] Liu P, Li CY, Wang Y, Fu YF. Climatic characteristics of convective and stratiform precipitation over the tropical and subtropical areas as derived from TRMM PR. Science China Earth Sciences. 2012;**56**:375-385

[20] Geerts B, Dejene T. Regional and diurnal variability of the vertical structure of precipitation systems in Africa based on spaceborne radar data. Journal of Climate. 2005;**18**:893-916

[21] Saikranthi K, Rao TN, Radhakrishna B, Rao SVB. Morphology of the vertical structure of precipitation over India and adjoining oceans based on long-term measurements of TRMM PR. Journal of Geophysical Research – Atmospheres. 2014;**119**:8433-8449

[22] Cao Q, Qi Y. The variability of vertical structure of precipitation in Huaihe River basin of China: Implications from long-term spaceborne observations with TRMM precipitation radar. Water Resources Research. 2014;**50**(5):3690-3705

[23] Marzuki M, Kozu T, Shimomai T, Randeu WL, Hashiguchi H, Vonnisa M. Raindrop size distributions of convective rain over equatorial Indonesia during the first CPEA campaign. Atmospheric Research. 2010;**96**:645-655

[24] Kozu T, Reddy KK, Mori S, Thurai M, Ong JT, Rao DN, Shimomai T. Seasonal and diurnal variations of raindrop size distribution in Asian monsoon region. Journal of the Meteorological Society of Japan. 2006;**84A**:195-209

[25] Tabata Y, Hashiguchi H, Yamamoto MK, Yamamoto M, Yamanaka MD, Mori S, Syamsudin F, Manik T. Observational study on diurnal precipitation cycle in equatorial Indonesia using 1.3-GHz wind profiling radar network and TRMM precipitation radar. Journal of Atmospheric and Solar - Terrestrial Physics. 2010;**73**(9):1031-1042

[26] Kumagai H, Masuda Y, Itabe T. Remote sensing in the troposphere and stratosphere. In: Okamoto K, editor. Global Environment Remote Sensing. 1st ed. Tokyo: Ohmsha Ltd; 1999. pp. 166-169

[27] Hazenberg P, Leijnse H, Uijlenhoet R. The impact of reflectivity correction and accounting for raindrop size distribution variability to improve precipitation estimation by weather radar for an extreme low-land mesoscale convective system. Journal of Hydrology. 2014. DOI: 10.1016/j.jhydrol.2014.09.057

[28] Kummerow C, Coauthors. The status of the tropical rainfall measuring mission (TRMM) after two years in orbit. Journal of Applied Meteorology. 2000;**39**:1965-1982

[29] Awaka J, Iguchi T, Okamoto K. TRMM PR standard algorithm 2A23 and its performance on bright band detection. Journal of the Meteorological Society of Japan. 2009;**87A**:31-52

[30] Marzuki M, Hashiguchi H, Yamamoto MK, Yamamoto M, Mori S, Yamanaka MD, Carbone RE, Tuttle JD. Cloud episode propagation over the Indonesian maritime continent from 10 years of infrared brightness temperature observations. Atmospheric Research. 2013;**120-121**:268-286

[31] Aldrian E, Susanto D. Identification of three dominant rainfall regions within Indonesia and their relationship to sea surface temperature. International Journal of Climatology. 2003;**23**:1435-1452

[32] Cao Q, Hong Y, Gourley JJ, Qi Y, Zhang J, Wen Y, Kirstetter P. Statistical and physical analysis of the vertical structure of precipitation in the mountainous west region of the United States using 11+ years of spaceborne observations from TRMM precipitation radar. Journal of Applied Meteorology and Climatology. 2013;**52**:408-424

[33] Marzuki M, Randeu WL, Kozu T, Shimomai T, Hashiguchi H, Schönhuber M. Raindrop axis ratios, fall velocities and size distribution over Sumatra from 2D-video disdrometer measurement. Atmospheric Research. 2013;**119**:23-37. In: Advances in Precipitation Science, edited by: Michaelides S

[34] Yin Y, Levin Z, Reisin T, Tzivion S. Seeding convective clouds with hygroscopic flares: Numerical simulations using a cloud model with detailed microphysics. Journal of Applied Meteorology. 2000;**39**:1460-1472

[35] Naumann AK, Seifert A. Recirculation and growth of raindrops in simulated shallow cumulus. Journal of Advances in Modeling Earth Systems. 2016;**8**:520-537. DOI: 10.1002/2016MS000631

[36] Takahashi H, Lebsock M, Suzuki K, Stephens G, Wang M. An investigation of microphysics and subgrid-scale variability in warm-rain clouds using the A-train observations and a multiscale modeling framework. Journal of Geophysical Research – Atmospheres. 2017;**122**:7493-7504

[37] Marzuki M, Kozu T, Shimomai T, Randeu WL, Hashiguchi H, Shibagaki Y. Diurnal variation of rain attenuation obtained from measurement of raindrop size distribution in equatorial Indonesia. IEEE Transactions on Antennas and Propagation. 2009;**57**:1191-1196